SIMULATING ATMOSPHERIC TURBULENCE USING A BUBBLE MODEL FOR FREE SPACE OPTICAL COMMUNICATION LINKS

by

Demet Yüksel

B.S., Electrical and Electronics Engineering, Bahçeşehir University, 2009

Submitted to the Institute for Graduate Studies in
Science and Engineering in partial fulfillment of
the requirements for the degree of
Master of Science

Graduate Program in Electrical and Electronics Engineering
Boğaziçi University

2013

SIMULATING ATMOSPHERIC TURBULENCE USING A BUBBLE MODEL FOR FREE SPACE OPTICAL COMMUNICATION LINKS

APPROVED BY:

Assist. Prof. Heba Yüksel (Thesis Supervisor)	.....
Prof. Emin Anarım	.....
Prof. Naci İnci	.....

DATE OF APPROVAL: 06.12.2013

ACKNOWLEDGEMENTS

First of all, I would like to thank to my advisor Assistant Professor Dr. Heba Yüksel for her excellent guidance, motivation and constant encouragement and for her invaluable support and meritorious comments on simulations. I am indebted to her for her inestimable help on my academic career.

Furthermore, I am also deeply grateful to my friend Melih Ahmet Karaman from Boğaziçi and Koç University for devoting extra time for his comments on simulations, his tireless support, guidance and reviews.

I am immensely grateful to my family. I can not thank enough my parents, Halil Yüksel, Gülnaz Yüksel and my siblings, Mehmet Edip Yüksel, Şeyma Yüksel, Fatma Yüksel, Elif Yüksel, İbrahim Yüksel, Emine Yüksel, Şeyma Yüksel and İsmail Yüksel for their endless love and support throughout my everlasting studies.

Additionally, I would like to thank Prof. Emin Anarım, and Prof. Naci İnci for being a part of my thesis committee and for their kind attitude.

ABSTRACT

SIMULATING ATMOSPHERIC TURBULENCE USING A BUBBLE MODEL FOR FREE SPACE OPTICAL COMMUNICATION LINKS

Free space optical (FSO) communication has emerged as a viable technology for broadband wireless applications. FSO technology offers the potential of high bandwidth capacity over unlicensed optical wavelengths. On long-range FSO links, atmospheric turbulence causes intensity fluctuations, which degrades links performance. Optical signals propagating through the atmosphere are subject to random fluctuations in phase and amplitude. These fluctuations are caused by random temperature distributions in the atmosphere, which manifests themselves as a random index of refraction changes along the propagation path. In addition, experimenting on a free space optical communication system is rather tedious and difficult. The interference of plentiful elements affects the result and causes the experimental outcomes to have bigger error variance margins than they are supposed to have. Especially when we go into the stronger turbulence regimes the simulation and analysis of the turbulence induced beams require delicate attention [1]. For all these purposes, we propose a new geometrical model to assess the effects of turbulence on laser beam propagation. The atmosphere along the laser beam propagation path will be modeled as a spatial distribution of spherical bubbles with refractive index discontinuity statistically distributed according to various models. For each statistical representation of the atmosphere, the path of rays will be analyzed using geometrical optics. These Monte Carlo techniques will assess the phase of the beam as well as the aperture averaging effects at the receiver. An effective turbulence index C_n^2 can be determined by correlating beam wander behavior with the path length. The Monte Carlo analysis will be compared with the predictions of wave theory as well as with empirical results [2].

ÖZET

SERBEST-UZAY OPTİK İLETİŞİM HATLARI İÇİN BALONCUK MODELİ KULLANARAK ATMOSFERİK ÇALKALANTILARIN BENZEŞTİRİMİ

Serbest uzay optik (SUO) iletişim geniş bantlı kablosuz uygulamalarıiçin geçerli bir teknoloji olarak belirmiştir. SUO teknolojisi, lisanssız optik dalga boyları üzerinde yüksek bant genişliği kapasitesi potansiyelini sunmaktadır. Uzun menzilli SUO hatlarında atmosferik çalkantı, dalgalanmaların şiddetlenmesine sebebiyet vererek hat performansını düşürmektedir. Atmosferde yayılan optik işaretler faz ve genliklerinde rasgele dalgalanmalara maruz kalmaktadır. Bu dalgalanmalar, kendilerini yayılım yolu boyunca rasgele kırılma değişim indisi olarak ortaya çıkaran atmosferdeki rasgele sıcaklık dağılımından kaynaklanmaktadır. Dahası, serbst uzay optik iletişim sistemi üzerinde deney yapmak zahmetli ve zordur. Çokça elemanın sebep olduğu girişimler sonucu etkileyip, deneysel çıktıların beklendiğinden daha büyük hata değişim paylarına sahip olmasına sebebiyet vermektedir. Özellikle daha şiddetli çalkantı rejimlerine girdiğimizde,çalkantı tarafından uyarılmış ışınların tahlili ve benzeştirimi daha hassas dikkat gerektirmektedir [1].Tüm bu nedenlerden dolayı, çalkantının lazer huzmesi yayılımındaki etkilerini değerlendirebilmek için geometrik bir model ortaya atmaktayız. Lazer huzmesi yayılım yolu boyunca olan atmosferi, istatistiksel olarak çeşitli dağılım modellerine uyacak kırılma indisi devamsızlığı olan küresel kabarcıkların uzaysal dağılımı olarak modellenecektir. Atmosferin her bir istatiksel temsili için, ışınların yolu geometrik optik kullanılarak tahlil edilecektir.Bu Monte Carlo teknikleri huzmenin fazını ve alıcıdaki ortalama açıklık etkilerini değerlendirebilmemizi sağlayacaktır. Etkin bir çalkalantı indisini, C_n^2 yol uzunluğu ve ışın sapmasıyla ilitinli kurarak ifade edebilriiz. Bu Monte Carlo çözümlemeleri, dalga kuramları öngörülerinin ve deneysel sonuçlarlada karşılaştırılabilir [2].

TABLE OF CONTENTS

LIST OF FIGURES

LIST OF TABLES

LIST OF ACRONYMS/ABBREVIATIONS

FSO	Free space optical
RF	Radio Frequency
LPI	Low Probability of Interception
LPd	Low Probability of Detection
Re	Reynolds Number
OPL	Optical Path Length
OPD	Optical Phase Difference
OPS	Optical Phase Shift
3D	Three Dimensional

1. INTRODUCTION

1.1. Overview of Free Space Optical Communication

Telecommunications systems have improved rapidly in order to meet the requirements of high data rate, voice, and video transmission. Radio communication systems and optical communication systems are two of the well-known systems for transmitting data. Optical communication systems provide higher speeds of data transmission, wider and license free spectrum, and are much more reliable than radio communication systems owing to the difficulty of intercept and low power requirements. Beside these advantages of Free Space Optics (FSO), there are some challenges of these systems. Atmospheric effects and the bad weather conditions like fog, rain, cloud, and snow influence performance of FSO systems adversely. In addition, line of sight path is required for FSO link because a laser beam cannot penetrate into obstructions such as walls, buildings, trees, and other materials that do not permit the light inside. Therefore, communications with FSO should be over short distances. Table 1.1 summarizes the comparison of FSO and RF technologies.

1.2. Architecture of FSO Systems

Optical Wireless Communication, also known as Free Space Optical communication, has three subsystems that are illustrated in Figure 1.1 for the transmission and reception of information. These are transmitter, receiver, and channel. FSO systems use the laser to transmit data. There are several lasers such as gas, chemical, dye, metal-vapor, solid state, semiconductor lasers, etc. The most important properties of these transmitters are power and spot size because spot size influences beam divergence. On the receiver side, the turbulence-induced signal fluctuations cause intensity fluctuations of the received signal. The receiver detects the intensity of the wave. Intensity refers to the power transferred per unit area and it has units of watts per meter squared (W/m^2). Intensity of the wave over the receiver diameter determines the aperture-averaging factor. Although lasers operate in an unlicensed spectrum, these

Table 1.1. Comparison of FSO Links and RF links.

	FSO	**RF**
Date Rate	100 Mbps - 5 Gbps	1 Gbps
Network Architecture	Scalable and Flexible	Non-Scalable
Spectrum	28 THz - 1000 THz (Most common 'eye-safe' frequency is 194 THz (1550 nm))	3 kHz to 300 GHz
Security	Low probability of interception or detection (LPI/LPD)	Directional RF: LPI/LPD Broadcast RF: HPI/HPD
Component Dimension	Small	Large
Range	Up to 200 Km	Up to 200 Km
Operation	Need Line-of-sight, Good in light-moderate rain, Poor in fog or snow.	Poor in heavy rain.

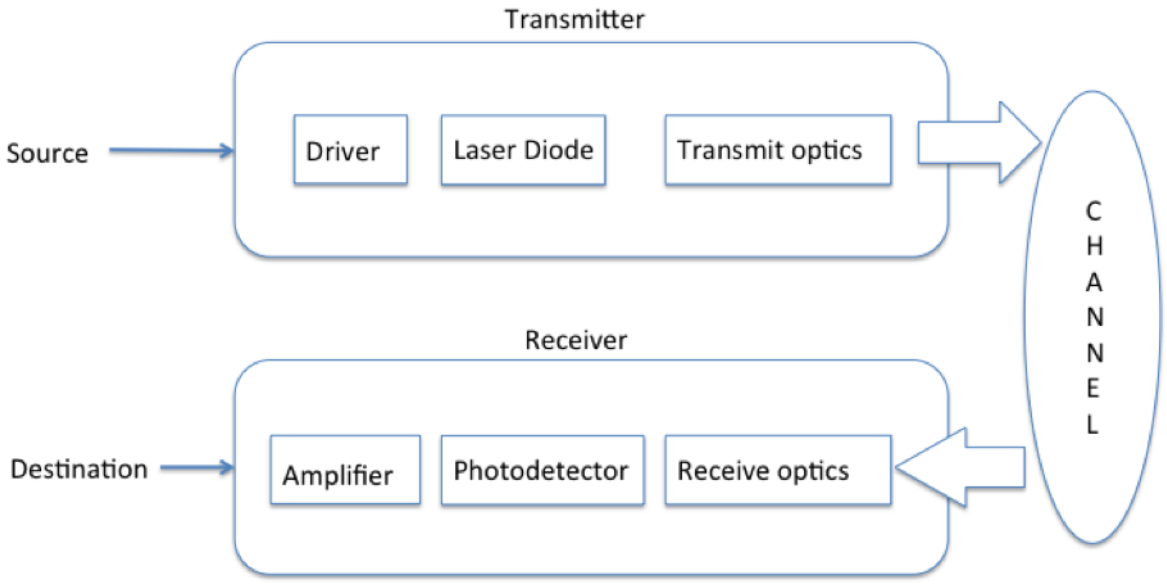

Figure 1.1. Block Diagram of FSO systems.

lasers use only short range of communication links because of the channel. Therefore, especially FSO systems are the most affected by the channel between the communication systems. This channel has several limitation factors that include bad weather conditions, obstructs and atmospheric turbulence. These factors degrade the received power of the laser beam but only obstacles eliminate the signal. Because of that, we examine the atmospheric channel in detail.

1.3. Atmospheric Channel

The fundamental effect of the FSO system is the atmospheric channel. The atmosphere is a dynamic medium with a randomly varying refractive index to a propagating laser beam. The resulting perturbations of the laser beam wavefront originating from space or being transmitted from the ground are broadly called atmospheric 'seeing' effects. Other effects include the irradiance fluctuations of the laser beams received and transmitted, beam wander, and spreading of the beam widths. These effects, and their impact on link performance, are discussed in Chapter 3.

When there is only weather condition and obstruction, we can easily calculate the effect of atmospheric channel over the power of receiving signal,

$$P_R = \frac{A}{\pi\theta^2 L^2} e^{-\alpha L} P_T \tag{1.1}$$

where P_R is the power of receiving signal for a receiver area A, range L, transmitted power P_T and beam divergence angle θ, and α is a constant value over the propagation path L. Obviously, when the transmitted power or receiver area is increased or the beam divergence angle of transmitter beam is decreased, the received power is increased. These increasing or decreasing of parameters are diffraction limited. This calculation is more complex in the presence of atmospheric turbulence. In this thesis, we especially focus on modeling atmospheric turbulence.

2. KEY INDICATOR of ATMOSPHERIC TURBULENCE

2.1. Turbulence Eddies

Atmospheric turbulence is caused by a temperature differential between the Earth's surface and atmosphere. This temperature difference in the atmosphere cause large-scale variations in the temperature of air. This process generates winds and as air moves with the winds, two distinct motions as a viscous fluid occurs. These are laminar and turbulent flow. In laminar flow, viscous forces are dominant and characterized by uniform or regular changes in velocity flow. In turbulent flow, viscous forces are dominant, and characterized by internal forces. Different temperature of air mixes so the velocity filed is unstable. This situation tends to produce randomly distributed pockets of air, called "turbulent eddies". These eddies have varying characteristic sizes and density. Because of this difference in the density of air, these eddies have different refractive indexes. Therefore, the atmosphere has a random refractive index profile. In the earliest study of turbulent flow, the Reynolds number (Re), a dimensionless quantity, has been used to characterize different flow regimes such as laminar or turbulent flow. Laminar flow occurs at low Reynolds numbers, whereas turbulent flow occurs at high Reynolds numbers. The Reynolds number is defined as

$$Re = \frac{\nu\iota}{\upsilon} \tag{2.1}$$

where ν is the characteristic velocity of the flow in units of m/s, l is the characteristic dimension of the flow in units of m and υ is the kinematic viscosity in units of m^2/s [7]. From the definition Equation 2.1, the Reynolds number grows according to the strength of turbulence. Reynolds numbers less that 2400 correspond to a laminar flow while those greater than 5000 correspond to turbulent flow [7]. In the view of Kolmogorov (1941), in turbulent flow, the kinetic energy in large eddies is transferred into smaller eddies as shown in Figure 2.2. This is known as the turbulent energy cascade. The average size of the largest eddies, L_0, is called the outer scale of turbulence. Near the ground, L_0 is on the order of the height above ground, while high above the ground,

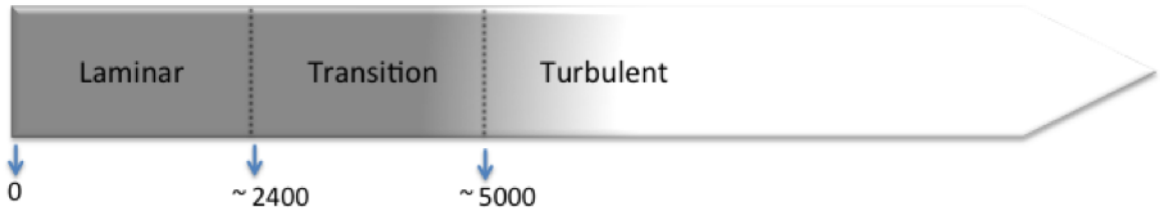

Figure 2.1. Diagram of Flow Regime.

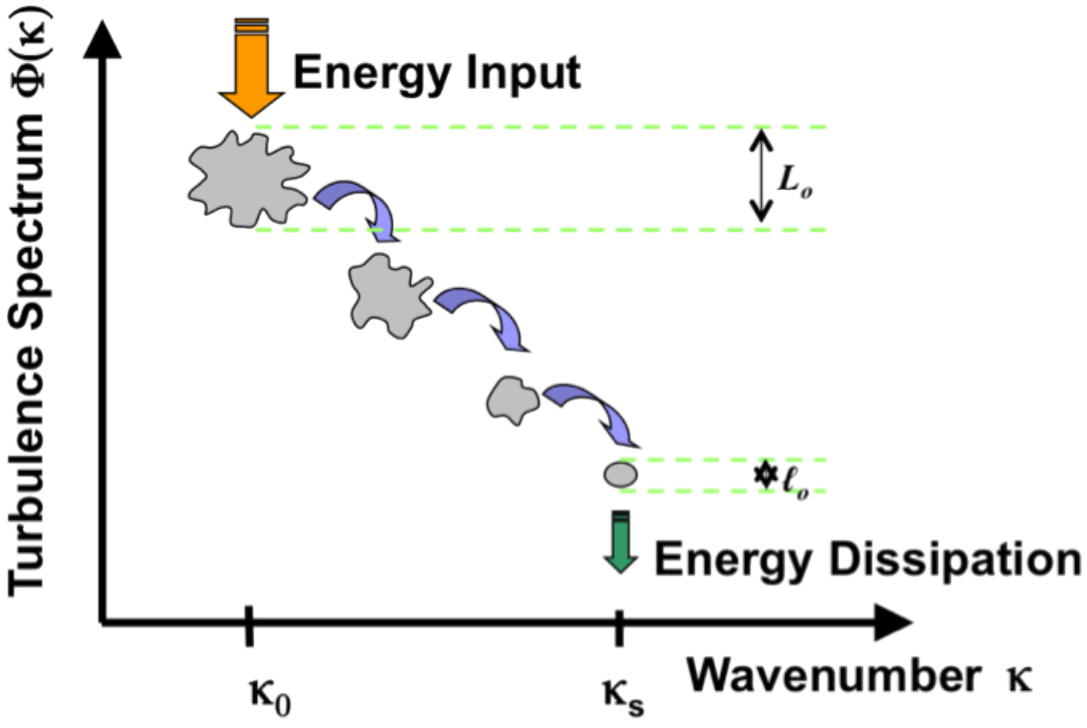

Figure 2.2. Kolmogorov theory of turbulence, where L_0 denotes the outer scale and l_0 is the inner scale. Eddies between scale sizes L_0 and l_0 form the inertial sub range [3].

it can be just tens to hundreds of meters. The average size of the smallest turbulent eddies, l_0, is called the inner scale. At very small scales, smaller than the inner scale, the energy dissipation caused by friction prevents the turbulence from sustaining itself. The inner scale, l_0, can be a few millimeters near the ground to a few centimeters high above the ground. Between inner and outer scales of turbulence, eddies are statistically homogeneous and isotropic. This means that properties such as refractive index and velocity have stationary increments. This range of scales is called the inertial sub-range. If the scale is smaller than the inner scale, the eddies are in the viscous dissipation range and if the scale is bigger than the outer scale, the eddies are not independent of parent flow [8].

According to research (2009), the inner scale, l_0, is between 2.7 to 4.3 cm, which approximates to that near ground levels and the uncertainty of measurement was less than 5% [9].

2.2. Refractive Index

As mentioned before, the atmosphere has a random refractive index profile. The small changes in the refractive index of the Earth's atmosphere are responsible for random fluctuations in the signal-carrying laser beam intensity (irradiance) called scintillation. Related turbulence-induced effects include beam spreading beyond the spreading predicted by diffraction (which decreases spatial power density incident on the receiver), and a continuous random motion of the beam centroid about the receiver (beam wander). Other significant effects of these refractive index fluctuations are aperture averaging, spatial coherence, angle of arrivals, absorption, and scattering. All of these affect directly the arrival point of the laser beam at the receiver. Beam wander, aperture averaging, Optical Path Length (OPL), Optical Phase Differences (OPD) and Optical Phase Shift (OPS) are very important terms for our simulation. They will be explained in more detail in upcoming sections.

Andrews described fluctuations caused by the changing refractive index [7]. Also Ishimaru had a similar description that the reflective particles are randomly distributed

in the medium and the medium scatters the laser propagated through [4]. The index of reflection fluctuations can be mathematically defined by n(R,t) [7]:

$$n(R,t) = n_0 + n_1(R,t) \tag{2.2}$$

where R is the point in space and t is the time parameter, $n_0 =< n(R,t) >= 1$ is the mean value of the refractive index and $n_1 = (R,t)$ represents the random deviation of n(R ,t) from its mean value. Therefore, $< n_1(R,t) >= 0$ so that the overall refractive index has a unit mean. Time variations are often suppressed in the refractive index for optical wave propagation. This means that the wave maintains a single frequency as it propagates. In the atmosphere, Equation 2.2 can be expressed as,

$$n(R) = n_0 + n_1(R) \tag{2.3}$$

where n(R) has been normalized by its mean value n_0. Fluctuations in the refractive index are related to corresponding temperature and pressure fluctuations. In particular, the refractive index of atmosphere n at a point R in space for optical wavelengths can be approximated as follows [7],

$$n(R) = 1 + 79 \times 10^{-}6\frac{P_R}{T_R} \tag{2.4}$$

where P is the pressure in millibars and T is the temperature in Kelvin.

2.3. Turbulence Theory Overview

Theoretical studies of optical wave propagation are traditionally classified as belonging to either weak or strong fluctuation theories based on the value of the Rytov variance defined as,

$$\sigma_1^2 = 1.23C_n^2k^{\frac{7}{6}}L^{\frac{11}{6}} \tag{2.5}$$

where C_n^2 is the refractive index structure parameter. The Rytov variance represents the intensity fluctuations (scintillation index) associated with an unbounded plane wave that has propagated a distance L. Weak fluctuation conditions are associated with $\sigma_1^2 < 1$ and strong fluctuations conditions with $\sigma_1^2 >> 1$, also known as saturation. Physically, the refractive index structure parameter C_n^2 is a measure of the strength of the fluctuations of the refractive index. By using optical devices such as a scintillometer, we can directly estimate the value of C_n^2 [10,11]. Optical turbulence in atmosphere can be characterized by three parameters. These are outer scale, L_0, inner scale, l_0, and the structure parameter of refractive index fluctuations, C_n^2. Refractive index structure parameter is a measure of the strength of the optical turbulence. The refractive index structure parameter is considered the most critical parameter along the propagation path in characterizing the effects of atmospheric turbulence. It is usually defined as the proportionality constant in the refractive index structure function. Therefore, C_n^2 is also called the structure constant. For statistically homogeneous and isotropic turbulence, the refractive index structure function D_n exhibits the asymptotic behavior,

$$D_n(R) = C_n^2 R^{2/3} \tag{2.6}$$

There are four different spectrums, which are defined differently according to wavenumber properties. These are Kolmogorov spectrum, Tatarski Spectrum, Von Karman Spectrum and Modified Atmospheric Spectrum. Kolmogorov defined the power spectral density for refractive index fluctuations over the inertial range by [7]:

$$\Theta_n(\kappa) = 0.033 C_n^2 \kappa^{-11/3}, \frac{1}{L_0} \leq \kappa \leq \frac{1}{l_0} \tag{2.7}$$

where κ is wave number ($\kappa = 2\pi/eddysize$). The Kolmogorov spectrum is used when the inner scale is zero and the outer scale is infinite, or as long as the wave number is within the inertial subrange. Tatarski defined the power spectral density for refractive index fluctuations over the dissipation range $\kappa \leq \frac{1}{l_0}$ by [7]:

$$\Theta_n(\kappa) = 0.033 C_n^2 \kappa^{-11/3} exp(-\kappa^2/\kappa_m^2), \kappa \geq \frac{1}{L_0} \tag{2.8}$$

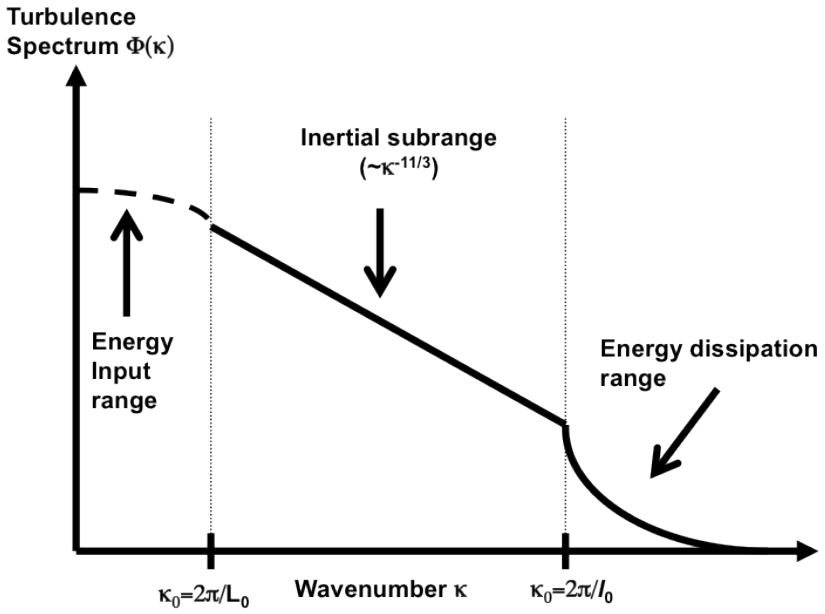

Figure 2.3. Spectrum of the refractive index fluctuation. The energy input range, Inertial subrange, and energy dissipation ranges are indicated [4].

where $\kappa_m = 5.92/l_0$. Von Karman modified the Tatarski spectrum such that it is finite for $\kappa \geq \frac{1}{L_0}$ to make it valid over both the inner and outer scale parameters,

$$\Theta_n(\kappa) = 0.033 C_n^2 \kappa^{-11/3} exp(-\kappa^2/\kappa_m^2), \kappa \geq \frac{1}{L_0} \tag{2.9}$$

where $\kappa_0 = 1/L_0$ (or $\kappa_0 = 2\pi/L_0$). Within the inertial subrange, both Tatarski and Von Karman spectra reduce to the Kolmogorov spectrum. Both the Tatarski and Von Karman spectra are based on mathematical convenience, not physical models [7].

3. GEOMETRICAL SIMULATION MODEL

3.1. Introduction

Free-space optical communication systems provide higher speeds of data transmission, wider license free spectrum, and are much more reliable owing to the difficulty of interception and the low power requirements. The main drawback of FSO systems is atmospheric turbulence. Therefore, since the 1960s, many scientists have been studying the effects of atmospheric turbulence on optical wave propagation [4, 12, 13]. Recently, the new term for FSO systems is full-optical free space optical communication systems since using full-optical free space communication systems is the best way to improve the communication speed [14, 15]. The main differences between full optical FSO and FSO systems are at the receiver side. Full-optical FSO systems have a fiber termination point instead of photo detectors [16]. Because of the new advances of FSO systems, estimating the atmospheric turbulence effect on the optical wave propagation through atmosphere turbulence becomes more important. There are many studies regarding the analysis of atmospheric turbulence effects on FSO systems but these studies analyze only some effects of atmospheric turbulence such as the strength of atmospheric turbulence (C_n^2), beam wander, angle of arrival or aperture averaging [14, 16, 17]. Our simulation model is based on an existing model of generating atmospheric turbulent eddies using geometrically generated spherical bubbles [6]. The main difference of our new model is that the bubbles are generated randomly with certain coverage percentages. Then generated environment is saved and the beam is propagated through the simulated media to calculate different parameters. Using our new model, we can effectively control the level of turbulence by adjusting the coverage percentages of the bubbles as well as their refractive indexes. This new geometrical simulation model is capable of assessing aperture-averaging, phase shift and beam wander for different atmospheric regimes. Our new model results are more consistent than the existing model especially for the aperture averaging and phase shift parameters.

3.2. Spherical Bubble Model

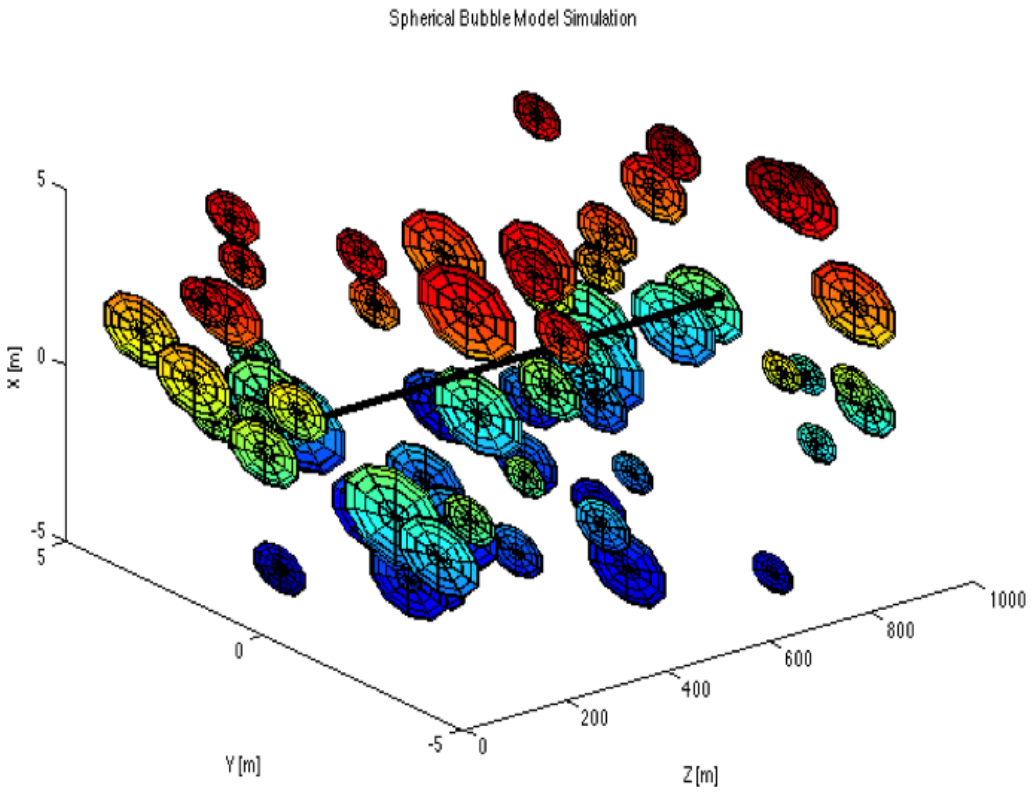

Figure 3.1. Spherical Bubble Model in Matlab Simulation.

The Spherical Bubble Model allows us to understand the effects of turbulence on laser beam propagation. This model includes a spatial distribution of spherical bubbles along the laser beam propagation path, which represent actual atmospheric eddies. The size and refractive index discontinuities represented by each bubble are statistically distributed according to various models. For each statistical representation of the atmosphere, the path of a single ray, or a bundle of rays, is analyzed using geometrical optics. These Monte Carlo techniques allow us to assess beam wander, beam spread, and phase shifts along the path. An effective C_n^2 can be determined by correlating beam wander behavior with the path length. This model has already proved capable of assessing beam wander, in particular the $(Range^3)$ dependence of mean-squared beam wander, and in estimating lateral phase decorrelations that develop across the laser phasefront as it propagates through turbulence. A Ray Interface Model,

which is a geometrical simulation model, was modeled by Walid Atia [6]. This model does not represent real eddy structure formation in the atmosphere because of their structure, which are curved interfaces. However, the new bubble model allows us to control the coverage percentage of the bubbles, which better describes the real eddy structure formation in the atmosphere. The sizes of the bubbles are chosen from a uniform distribution with a minimum diameter of 1 mm representing the inner scale of turbulence, l_0, and a maximum value of 1 m representing the outer scale of turbulence, L_0. The refractive indexes of the bubbles are chosen from a Gaussian distribution with a mean value corresponding to the index of air, which has been taken in the simulation from an experimental result [18]. Therefore, the mean index of refraction is taken as $\mu_n = 1.00026$ and the standard deviation as $\sigma_n = 0.000016$. Figure 3.1 illustrates the Spherical Bubble Model.

3.2.1. Geometrical Analysis of Atmospheric Turbulence Simulation Model

In describing the procedure of our model, we make use of some of the described geometrical structures used in Heba Yuksel's existing model [5] with emphasis on the difference between the two techniques. The geometrical analysis is described in detail since it will be used in all of the simulations for calculating beam wander, aperture averaging, Optical Path Length (OPL), Optical Phase Differences (OPD), and Optical Phase Shift (OPS) in this chapter [6].

The uniform and Gaussian (normal) distributions will be used in the simulation model to evaluate the refractive indices and sizes of the spheres. For this reason, their definition is defined before generating the spheres [5].

A uniform distribution in the range of [0, 1], which we call here U(0,1) simply returns a number within the specified range with equal probability. In order to modify such a distribution to increase the range, a multiplicative constant needs to be applied to the uniform distribution, U(0,1). In addition, the end points can simply be modified by adding and subtracting the appropriate values to the random uniform distribution

[5].

$$f(\chi) = \frac{1}{\sigma\sqrt{2\pi}} exp\left[-\frac{1}{2}\left(\frac{\chi-\mu}{\sigma}\right)^2\right] for -\infty \leq \chi \leq \infty \tag{3.1}$$

where μ is the mean, σ^2 is the variance, and χ here is said to possess a normal distribution which we denote here as $N(\mu, \sigma^2)$. A normal distribution can be obtained using several methods, one of which is described in detail by Morgan [19]. Morgan has defined a method of forming a normal distribution from two uniform distributions. If we call the uniform distributions, V1 = U(-1,1) and V2 = U(-1,1), then we can generate a pair of independent normal variables with zero mean and unit variance from the relation [19],

$$N_1 = V_1\left(\frac{-2lnW}{W}\right)^{\frac{1}{2}}, \tag{3.2}$$

$$N_2 = V_2\left(\frac{-2lnW}{W}\right)^{\frac{1}{2}}, \tag{3.3}$$

where $W = V_1^2 + V_2^2$. To generate a normal variable with mean μ other than zero, we can simply add μ to N_1 and N_2. To create a normal variable with standard deviation σ, we need to multiply the standard normal by σ.

The three-dimensional space is first filled with spherical bubbles of varying size ranging between 1 mm and 1 m. There is a coverage percentage chosen for the percentage of bubbles filling the three-dimensional space. The bubbles are chosen such that they do not intersect or touch each other. The bubbles are then sorted by the z-coordinates of their centers. The starting x and y coordinates of the rays (x_0, y_0) are each selected from a random Gaussian distribution with means $(\mu_x = 0)$, $(\mu_y = 0)$, respectively and variance $\sigma^2 = w^2$, where w is the beam spot size at the transmitter (starting point) taken as 20 mm. The starting z-coordinate of all of the rays is at z=0.

After filling the space with spheres by using uniform and gaussian distributions, the second part is to solve the intersection point between the incident ray and the sphere. Each ray is checked for intersection with any of the bubbles and the bubble with the smallest z-coordinate is chosen for the ray to refract through it according to Snell's law. Such a check is done until no more spheres can be intersected by the ray within the chosen three-dimensional space. Then, the ray is made to propagate to the target length L. This can be done by solving the sphere equation with the ray vector equation. The line equation can be defined as,

$$\frac{x_2 - x_1}{l} = \frac{y_2 - y_1}{m} = \frac{z_2 - z_1}{n}, \tag{3.4}$$

where (x_1, y_1, z_1) and (x_2, y_2, z_2) are 2 points on the line, and l, m, n are the directional cosines of the line. The directional cosines are defined as $l = cos\alpha$, $m = cos\beta$, $n = cos\gamma$, where α, β, γ are the angles that the vector makes with the positive $x-, y-, z-$axes, respectively. In addition, we have the following inequality,

$$cos^2\alpha + cos^2\beta + cos^2\gamma = 1. \tag{3.5}$$

The sphere equation is defined as,

$$(x_2 - x_0)^2 + (y_2 - y_0)^2 + (z_2 - z_0)^2 = R^2, \tag{3.6}$$

where (x_2, y_2, z_2) is a point on the sphere, (x_0, y_0, z_0) is the center of the sphere and R is the radius of the sphere. A solution is checked for z_2 in Equation 3.4 into Equation 3.6. If a solution exists, the smaller root of z_2 is taken from which x_2 and y_2 can be solved for. The other part of the simulation procedure is applying the three-dimensional Snell's law to calculate the refracted vector.

A three-dimensional Snell's law is applied to calculate the refracted output vector given the incident vector and the normal to the sphere. When a ray traveling in free-space encounters a dielectric interface, it refracts due to the change of index

it encounters. The boundary conditions state that the tangential component of the electric field and the normal component of the magnetic field are continuous. In order to satisfy such conditions, Snell's law defines the relation between the incident and refracted angle as follows,

$$n_1 sin(\theta_1) = n_2 sin(\theta_2), \tag{3.7}$$

where n_1 and n_2 are the indices of refraction of air and the sphere respectively when the ray is entering the sphere and reversely when the ray is exiting the sphere. θ_1 and θ_2 are the incident and refracted angles with the normal to the spheres, respectively. In addition, the boundary conditions require that the refracted ray $\overrightarrow{r_2}$ to lie in the same plane as the plane of incidence which includes the incident ray $\overrightarrow{r_1}$ and the normal to the sphere $\overrightarrow{n}$. We define $\overrightarrow{P_1}$ to be the perpendicular vector to the plane of incidence with magnitude $\sin(\theta_1)$ and $\overrightarrow{P_2}$ to be in the same direction as $\overrightarrow{P_1}$ but with magnitude $\sin(\theta_2)$. If we use unit vectors for the incident ray ($\widehat{r_1}$), refracted ray ($\widehat{r_2}$) as well as the sphere's normal ($\widehat{n}$), then we can write $\overrightarrow{P_1}$ and $\overrightarrow{P_2}$ as,

$$\overrightarrow{P_1} = \widehat{r_1} \times \widehat{n}, \tag{3.8}$$

$$\overrightarrow{P_2} = \widehat{r_2} \times \widehat{n}. \tag{3.9}$$

Given the incident ray $\widehat{r_1}$ and the sphere's normal $\widehat{n}$, $\overrightarrow{P_1}$ can be determined through Equation 3.8. The incident angle is then θ_1 where,

$$sin(\theta_1) = |\overrightarrow{P_1}|. \tag{3.10}$$

The refracted angle θ_2 can then be calculated through the application of Snell's law, Equation 3.7. Therefore, $\overrightarrow{P_2}$ is,

$$sin(\theta_1) = |\overrightarrow{P_1}|. \tag{3.11}$$

where $\widehat{P_1} = \overrightarrow{P_1}/|\overrightarrow{P_1}|$ is the normalized unit vector of $\overrightarrow{P_1}$. Figure 3.2 shows the three-dimensional Snell's Law which can be used to determine the refracted ray $\widehat{r_2}$. The refracted unit vector $\widehat{r_2}$ can be evaluated through adding the $\widehat{n} \times \overrightarrow{P_2}$ vector which is the plane of incidence to a scaled version (by a constant λ) of the unit vector of the sphere's normal $\widehat{n}$,

$$\widehat{r_2} = \lambda \widehat{n} + \widehat{n} \times \overrightarrow{P_2} \tag{3.12}$$

Therefore, in order to calculate the output vector $\widehat{r_2}$, we only need to know the incident vector, the normal to the sphere, and the refractive indices of the spheres assuming air of index 1.00016 between the spheres.

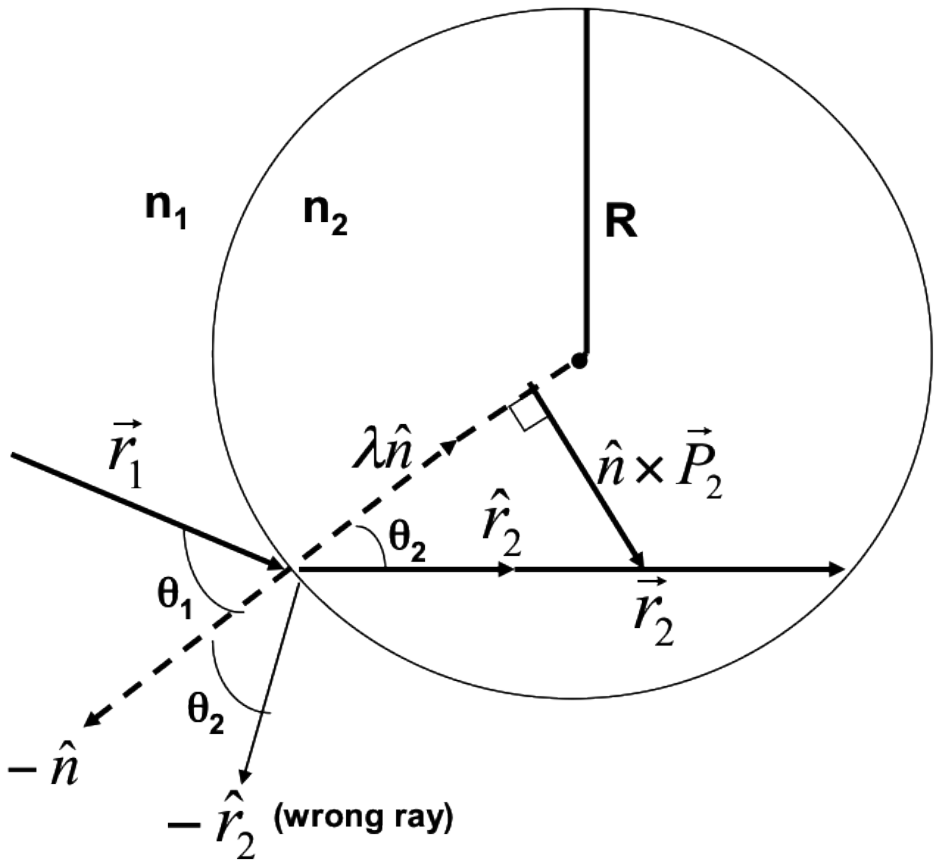

Figure 3.2. Three dimensional Snell's Law [5].

Equation 3.12 can be rewritten as

$$|\widehat{r_2}|^2 = |\widehat{n} \times \overrightarrow{P_2}|^2 + |\lambda\widehat{n}|^2 + 2|\lambda\widehat{n}| \cdot |\widehat{n} \times \overrightarrow{P_2}| \tag{3.13}$$

where $|\widehat{r_2}| = 1$. But the last term in Equation 3.13 is zero since the $\widehat{n}$ vector is perpendicular to the $\widehat{n} \times \overrightarrow{P_2}$ vector as shown in Figure 3.2. If we specify $\widehat{n} \times \overrightarrow{P_2} = [a, b, c]$ and $\widehat{n} = [n_x, n_y, n_z]$, then,

$$\lambda^2 + a^2 + b^2 + c^2 - 1 = 0. \tag{3.14}$$

Defining $\tilde{a} = 1$, $\tilde{b} = 2an_x + 2bn_y + 2cn_z = 0$ and $\tilde{c} = a^2 + b^2 + c^2 - 1$, and noting that $n_x^2 + n_y^2 + n_z^2 = 1$, the solution for λ can be written as,

$$\lambda = \frac{-\tilde{b} \pm \sqrt{\tilde{b}^2 - 4\tilde{a}\tilde{c}}}{2\tilde{a}}. \tag{3.15}$$

This equation yields two solutions for $\widehat{r_2}$, but only the solution that gives a positive z component is correct and is chosen. Using Figure 3.2, the unit vector $\widehat{r_2}$ can be multiplied by a scaling factor to determine the full refracted vector $\overrightarrow{r_2}$,

$$\overrightarrow{r_2} = \widehat{r_2} \cdot (2Rcos(\theta_2)), \tag{3.16}$$

where R is the radius of the sphere.

The last part of the simulation procedure is where a ray intersects the end point. This can be achieved through solving the ray's incident vector with the plane z=k, where k is the propagation path in the z-direction. For example, let us assume the incident unit vector for the ray to be (V_x, V_y, V_z), and its starting point as (x_1, y_1, z_1). Then the end point for the ray is,

$$(x_2, y_2, z_3) = (x_1 + V_x.t, y_1 + V_y.T, k), \tag{3.17}$$

where $t = (k - z_1)/V_z$.

3.2.2. Beam Wander

When an optical beam propagates through the atmosphere, turbulence eddies causes random deflection of the beam. Therefore, the beam centroid will wander randomly from the propagation direction. This wander can be characterized statistically by variance of the displacement or component along a single axis [20].

Chernov and Beckmann used a geometrical optics approach to calculate the wander of a single ray [12,21]. However, this formulation does not include the effects of the finite beam diameter. Andreev and Gelfer used a Huygens-Fresnel approach to calculate the beam wander of a Gaussian beam. They based the wander on the gradient of the refractive index along the beam, so that their calculation is equivalent to that of Chernov in that beam size effects are not considered [22]. They conclude incorrectly that the wander does not depend on the curvature of the initial beam.

The mean squared beam wander is defined by Ishimaru as [4],

$$< \rho_1^2 >= \frac{W_0^2}{2}[(\alpha_1 z)^2 + (1 - \alpha_2 z)^2] + 2.2 C_n^2 l_0^{\frac{-1}{3}} z^3, \tag{3.18}$$

where z is the propagation distance, l_0 is the inner scale, $\alpha_2 = 1/R_0$, where R_0 is the radius of the equivalent Gaussian wave, W_0 is the spot-size, and $\alpha_1 = \lambda/(\pi W_0^2)$. For plane waves, the equation for the mean square beam wander simplifies to [23],

$$< \rho_1^2 >= 2.2 C_n^2 l_0^{\frac{-1}{3}} z^3. \tag{3.19}$$

In our simulation, we will deal only with the plane wave case. Under the weak turbulence condition with $C_n^2 = 10^{-17}$ at the range of 1 km and $l_0 = 1mm$, the root-mean-square (RMS) beam wander is about 0.47 mm. Under the intermediate turbulence condition with $C_n^2 = 10^{-15}$ at the range of 1 km and $l_0 = 1mm$, the root-mean-square (RMS) beam wander is about 4.7 mm. Under the strong turbulence condition with

$C_n^2 = 10^{-13}$ at the range of 1 km and $l_0 = 1mm$, the root-mean-square (RMS) beam wander is about 47 mm.

3.2.2.1. Beam Wander Simulation Model. The atmosphere has a random refractive index profile. The small changes in the refractive index of the Earth's atmosphere are responsible for random fluctuations in the signal-carrying laser beam intensity (irradiance) called scintillation. Related turbulence-induced effects include beam spreading beyond the spreading predicted by diffraction (which decreases spatial power density incident on the receiver), and a continuous random motion of the beam centroid about the receiver (beam wander). We use the mean square beam wander equation for a plane wave, Equation 3.19, for calculating C_n^2.

Our simulation model calculates the three dimensional trajectory for a single ray or a bundle of rays traveling a distance L through a simulated random medium modeled as a series of random spheres/bubbles of random refractive index. For each statistical representation of the atmosphere, the path of a single ray or a bundle of rays is analyzed using geometrical optics. The mean square beam wander is averaged over many simulation runs. Figure 3.3 illustrates the beam wander simulation.

3.2.2.2. Measuring Turbulence Strength. The mean squared beam wander (Equation2.5) is calculated for varying σ_n values from beam wander simulation model. C_n^2 can then be calculated through the Rytov variance equation where the inner scale of turbulence l_o which represents the smallest sphere size is taken as 1 mm. Table 3.1 shows C_n^2 for varying coverage percentages of bubbles.

3.2.2.3. Beam Wander Simulation Results. Figure 3.4 plots the beam wander simulation results using the following parameters: L=1 km, $\mu = 1.00027$ (mean index of refraction for the spheres), $\sigma = 0.000016$, Nrays=1000 rays/simulation and Nrun=1000. The radius of the spheres is chosen in the range of 1 mm to 1 m. It is clear that the simulation results show excellent agreement with the cubic fit described in theory in Equation 3.19. In Fig 3.4, the cubic fit expected by theory is shown for the weak

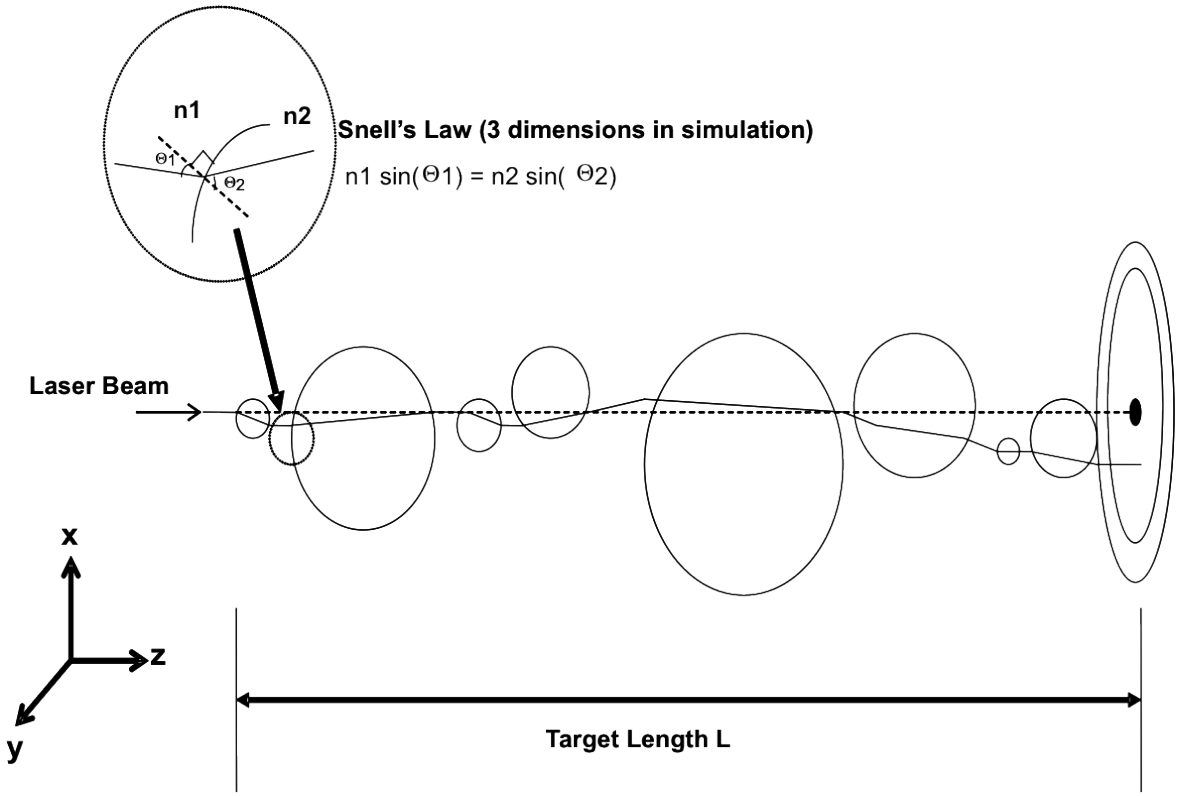

Figure 3.3. Beam Wander Simulation Model [6].

Table 3.1. C_n^2 for varying coverage percentage of bubbles.

Coverage Percentage of Bubbles	C_n^2 **(Strength of Atmospheric Turbulence)**	**Level of Turbulence Regime**
%30	1.10e-12	Strong
%3	5.91e-14	Intermediate
%0.2	9.92e-16	Weak

turbulence results.

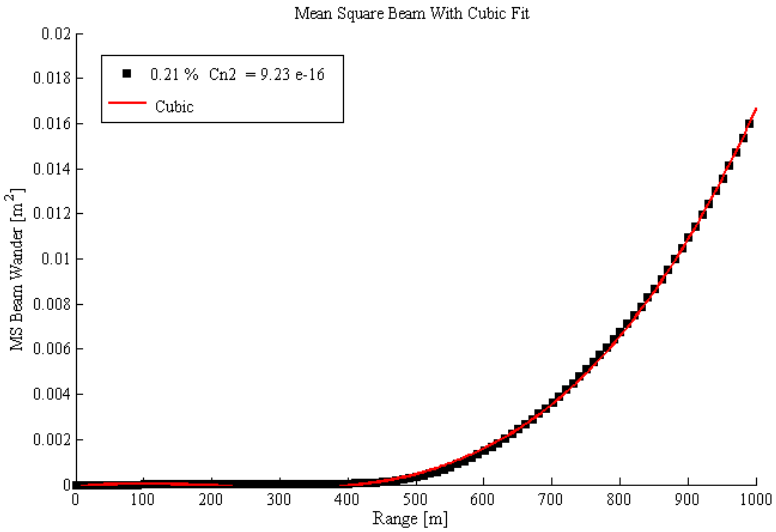

Figure 3.4. Mean Square Beam Wander Curve and Cubic Fit Curve for a 1 km range using the Spherical/Bubble Model .

Figure 3.5 reinforces the fact that as turbulence gets stronger, the Mean Square Beam wander gets significantly larger. A factor of 10 increase in C_n^2 gives almost a factor of 10 increase in the mean square beam wander.

Figure 3.6 shows the beam wander results for different turbulent regimes controlled by the bubble coverage percentages. It is clearly shown that the stronger the turbulence level, the greater the mean square beam wander.

3.2.3. Aperture Averaging Simulation Model

This model calculates the aperture-averaging factor for a number of rays propagating through turbulence simulated spherical bubbles into a circular receiver of varying aperture sizes. The three-dimensional trajectory of each ray is analyzed using geometrical optics. The numbers of rays that reach the target length L, within the selected receiver aperture size are summed. The variance of the total rays within each aperture size is then calculated over N simulation runs. Such variances are then normalized by

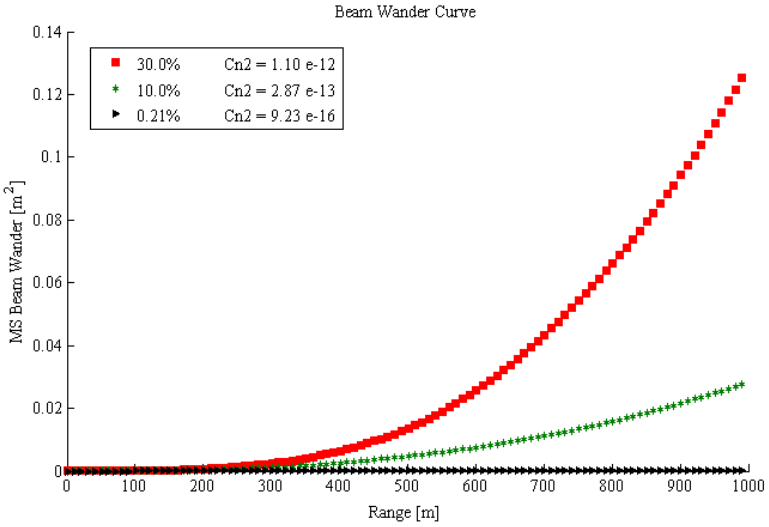

Figure 3.5. Mean Square Beam Wander Curves for Weak, Intermediate and Strong Turbulence.

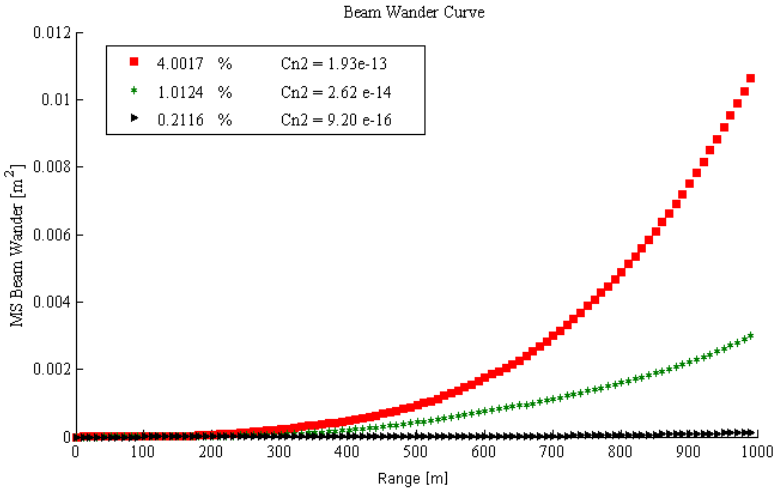

Figure 3.6. Mean Square Beam Wander Curves for Weak and Intermediate Turbulence.

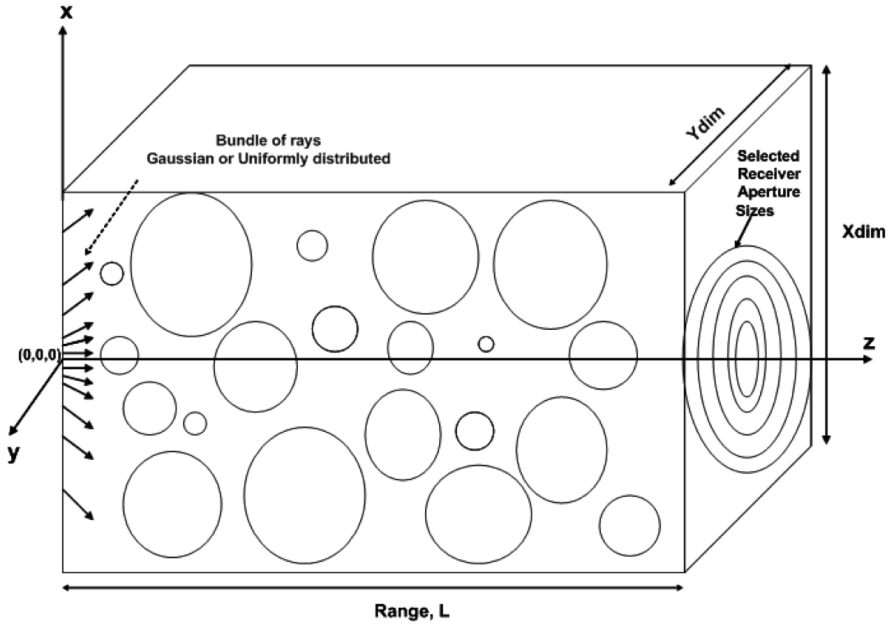

Figure 3.7. Aperture Averaging Simulation using the Spherical Bubble Model [5].

the variance of the smallest chosen aperture size to evaluate the aperture-averaging factor,

$$F = \frac{\sigma_I^2(D)}{\sigma_I^2(D=0)} \tag{3.20}$$

After the rays reach the receiver, each ray's beam wander from the center $\sqrt{x_2 + y_2}$ is checked for whether or not it lies within some selected circular aperture sizes at the receiver. If so, it gets counted. The same procedure is repeated for each of the rays. Then the whole simulation is repeated N times for different rays' distributions. The variance of the total rays within each aperture size is then calculated over the simulation runs. Such variances are then normalized by the variance of the smallest chosen aperture size to evaluate the aperture-averaging factor, F.

3.2.3.1. Aperture Averaging Simulation Results. The sample variance form is used in calculating the variance of for each particular aperture diameter over 1000 simulation runs. It is then normalized by the mean squared to calculate the normalized aperture-

averaged variance,

$$\sigma_{Ii}{}^2(D) = \frac{\frac{\sum(x_{ij}-\mu_i)^2}{N-1}}{\mu_i^2} \tag{3.21}$$

where i is the aperture diameter index and j is the simulation run index. Equation 3.21 is then divided by the normalized variance of the minimum aperture diameter to evaluate the aperture averaging factor F (Equation 3.20).

Through plugging Equation 3.21 in Equation 3.20, the aperture averaging factor is calculated and plotted in Figure 3.8 for weak, intermediate and strong turbulence regimes respectively. We change the coverage percentage of the bubbles to change the number of eddies in the simulated turbulent media, which changes the turbulent strength. Our results show the expected nonlinear reduction of the aperture-averaging factor with aperture diameter. The weaker the turbulence, the steeper the initial decline, and the faster saturation occurs.

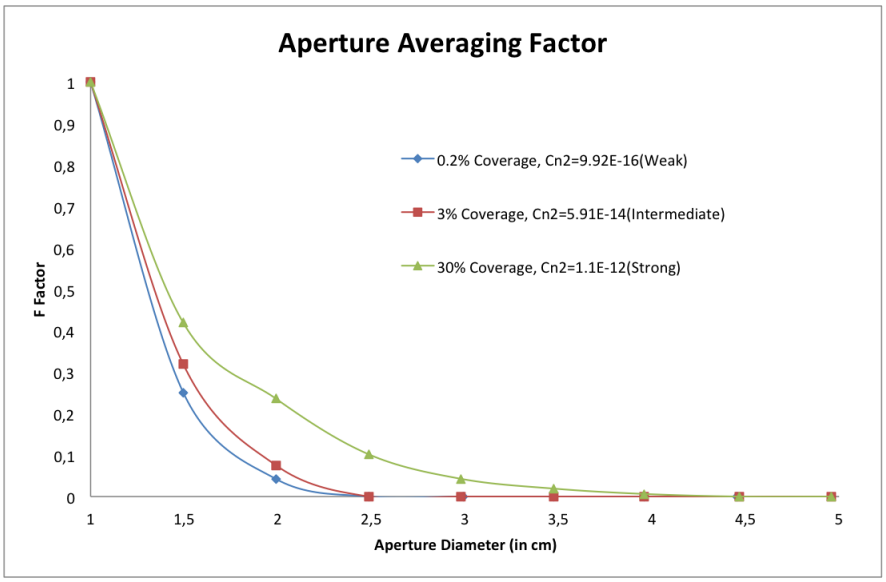

Figure 3.8. Aperture Averaging Factor F versus the aperture radius.

3.2.4. Optical Phase Difference Theory

A geometrical model for understanding the optical phase difference between two beams propagating through a simulated turbulent media as their separation distance is changed. Beam separations less than the inner of scale of turbulence should be very well correlated because these ranges are likely to be within the same eddy. Large separations should tend to become completely uncorrelated. The geometrical model can give us more insight into the correlation between two beams propagating in different atmospheric turbulent regimes as their separation distance is changed.

The mean square phase difference for a plane wave propagating through weak turbulence is equivalent to the phase structure function, $D_p(r)$. Only those eddies with scale sizes exceeding or on the order of the separation distance, r, contribute to any correlation, $l = \frac{2\pi}{\kappa} \geq r$. The phase structure function yields a relative phase difference for the plane wave [13],

$$D_p(r) = 0.64 C_n^2 k^2 L r^{\frac{5}{3}}. \tag{3.22}$$

If instead of a plane wave, we considered a pair of collimated parallel pencil thin beams separated by a distance r, Equation 3.22 would exactly result in,

$$D_p(r) = 0.32 C_n^2 k^2 L r^{\frac{5}{3}}. \tag{3.23}$$

The Optical Phase Difference (OPD) is proportional to the difference in the respective path lengths traversed by two rays, which are initially in phase. We calculate the Optical Path Length for a bundle of rays propagating through a simulated turbulent media. The Optical Path Length (OPL) traversed by a ray traveling a distance L in a medium of refractive index n is,

$$L = OPL = n_medium \cdot l_medium. \tag{3.24}$$

If light travels through 'm' different media, the total OPL is the sum of the optical paths in each of the different media:

$$L_{total} = OPL_{total} = n_1 l_1 + n_2 l_2 + \cdots + n_m l_m = \sum_{i=1}^{m} n_i l_i. \tag{3.25}$$

Then the Optical Phase Difference (OPD) $\Delta\phi$ of two rays, initially in phase, that have traversed optical path lengths L_1 and L_2, respectively, is:

$$\Delta\phi = \frac{2\pi}{\lambda}\Delta L, \tag{3.26}$$

where $\Delta l = L_1 - L_2$ is the optical path difference.

3.2.4.1. Optical Phase Difference Simulation Model. The trajectories of two parallel rays propagating through the simulated random medium are computed simultaneously. Figure 3.9 illustrates the OPD simulation procedure. The difference in the path length traveled ΔL will yield the phase difference $\Delta\phi$ between the rays using Equation 3.26. A single simulation run is comprised of the following steps: The user inputs the length of the target L, the mean index of refraction μ_n and standard deviation for the refractive index σ_n, the starting separation between the beams r and the step size between separations Δr, and the number of run desired N. Two beams are started out separated by a distance r at the coordinates (0,0,0) and (-r,0,0). The index of refraction of the spheres/bubbles for both beams is chosen from a Gaussian distribution. Similarly, the sphere's radius and center are chosen from a uniform distribution with the condition that the first propagating ray starting at (0,0,0) must hit the randomly generated sphere. A single path length is chosen from a Gaussian distribution, and two beams travel this length to intersect the sphere. Snell's law is then invoked to find each beam's new output vector. The square difference between the beams is then averaged and saved for the particular value of separation r, after which r is decremented by Δr and the simulation is restarted until r = 0 (for which $\Delta\phi = 0$). The beam separation was chosen to range from $10\lambda L = 25cm$ to 0 (no separation) assuming a He-Ne laser beam propagating with $\lambda = 632.8nm$.

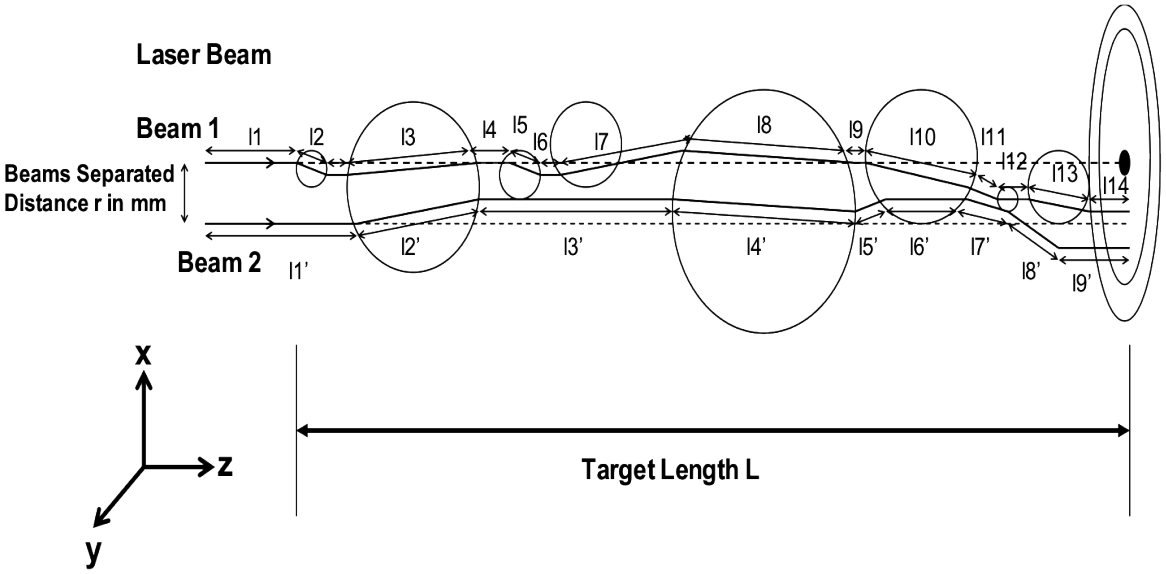

Figure 3.9. Optical Phase Difference Simulation Model [6].

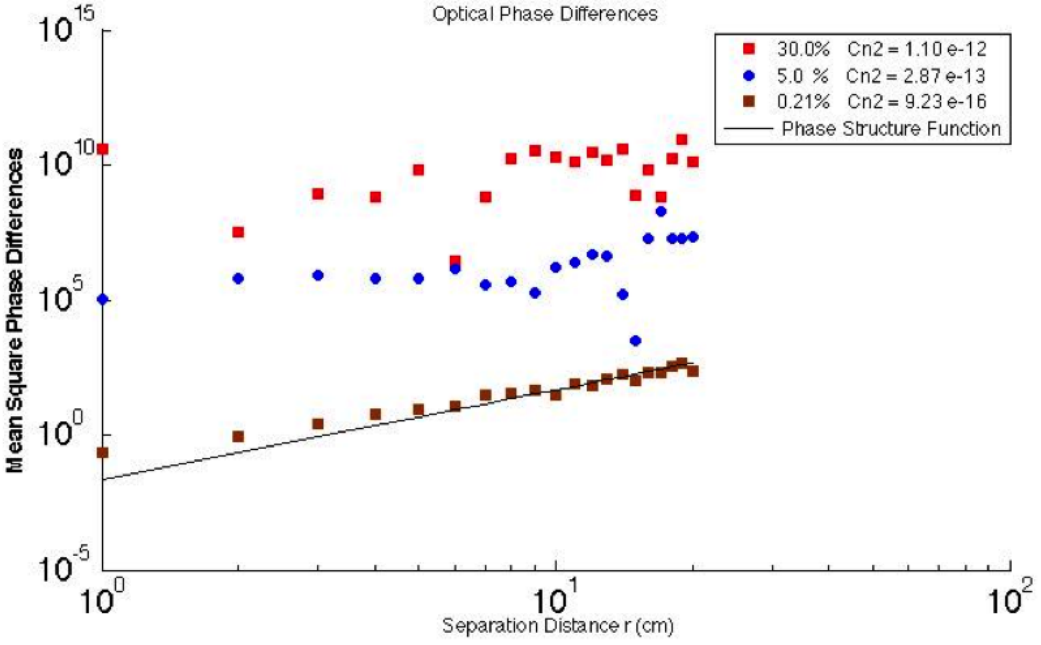

Figure 3.10. Optical Phase Difference and Phase Structure Function .

3.2.4.2. Optical Phase Difference Simulation Model Results. Figure 3.10 shows the mean square phase differences versus the separation distance, r. The weak turbulence data seem to follow the 5/3 slope predicted by theory. However, for very strong turbulence, at large separations, the two rays seem to show no correlation as expected. Therefore, for such conditions, in real FSO systems, the fluctuations are uncorrelated, but the data is correlated.

3.2.5. Optical Phase Shift Theory

This model calculate the OPL from Equation3.26 because after the EM wave travels through a certain optical path, we can calculate the optical phase shift (OPS) which is described by,

$\phi = 2\pi$ radians /cycle $\times$ number of cycles the wave has travelled

$$= 2\pi \frac{OPL}{\lambda} = 2\pi \frac{nl}{\lambda}, \tag{3.27}$$

where the wavelength of a He-Ne laser, $\lambda = 632.8nm$ is used in the simulation. If the beam travels through 'm' different media, the total "optical phase shift" is,

$$\phi_{total} = \frac{2\pi}{\lambda} OPL_{total} = \frac{2\pi}{\lambda} \cdot \sum_{i=1}^{m} n_i l_i. \tag{3.28}$$

3.2.5.1. Optical Phase Shift Simulation Model. The Optical Phase shift simulation model calculates the total phase shift of a bundle of rays propagating through the simulated turbulent media shown in Figure 1. For each statistical representation of the atmosphere, the path of a bundle of rays is analyzed using geometrical optics. The mean of the optical phase shift is calculated for 1000 rays and 1000 runs and the standard deviation of the total optical phase shift is calculated for 1 ray over 1000 runs.

Figure 3.11 illustrates the phase shift model.

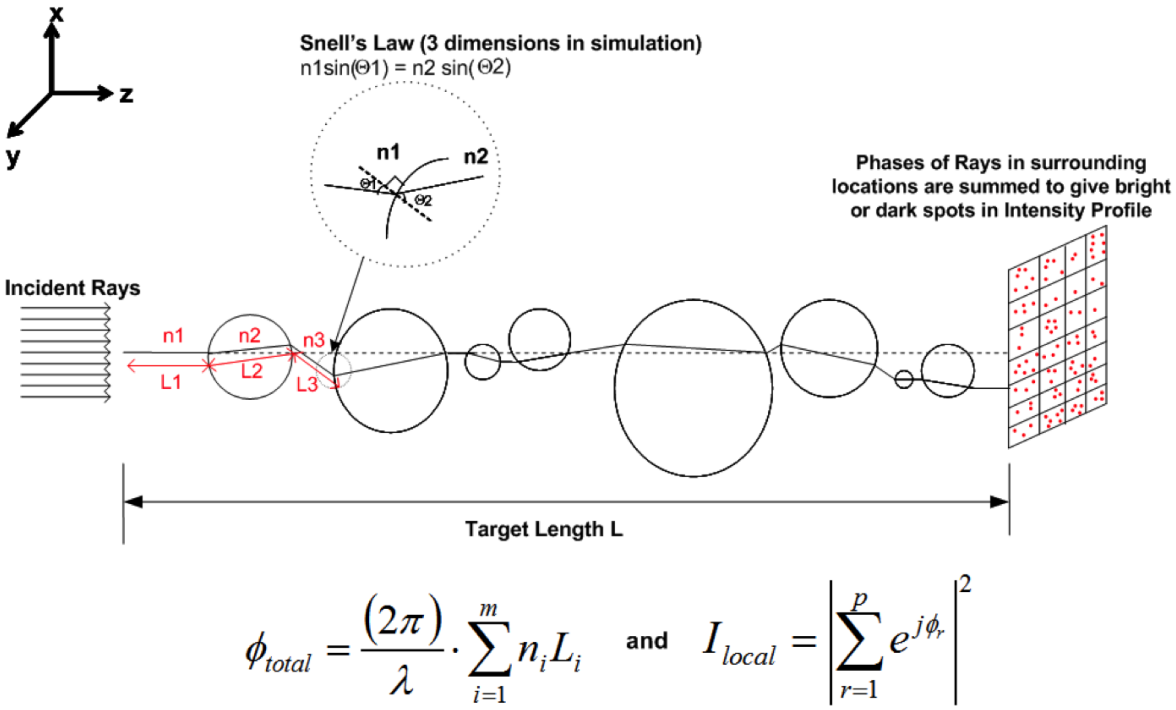

Figure 3.11. Optical Phase Shift Simulation Model.

3.2.5.2. Optical Phase Shift Simulation Results. A particular simulation run is comprised of the following: The user inputs the length of the target L, the mean index of refraction of the spheres μ_n taken as the air index and standard deviation for the refractive index σ_n, and the number of runs desired N. The index of refraction of the spheres is chosen from a Gaussian distribution, and the sphere's center and radius are chosen from a uniform distribution. The spherical bubbles are then formed using the above parameters for different chosen coverage percentages reflecting varying turbulence conditions. For every simulated media, the turbulence index parameter, C_n^2, is calculated using Equation 3.19 along with our beam wander simulation model introduced in our previous work [6]. A beam, formed of a bundle of rays uniformly distributed, is then started out at location (0,0,0) in the z-direction. Snell's law is then used to evaluate the new output vectors at the entering and exiting points of the spheres. The ray then travels through the simulated random medium and the opti-

cal path length is evaluated for each ray using Equation 3.28 until the target length is reached. The mean and standard deviation of the optical phase shift is updated, and the next run begins. Figure 3.12 plots the mean optical phase shift simulation

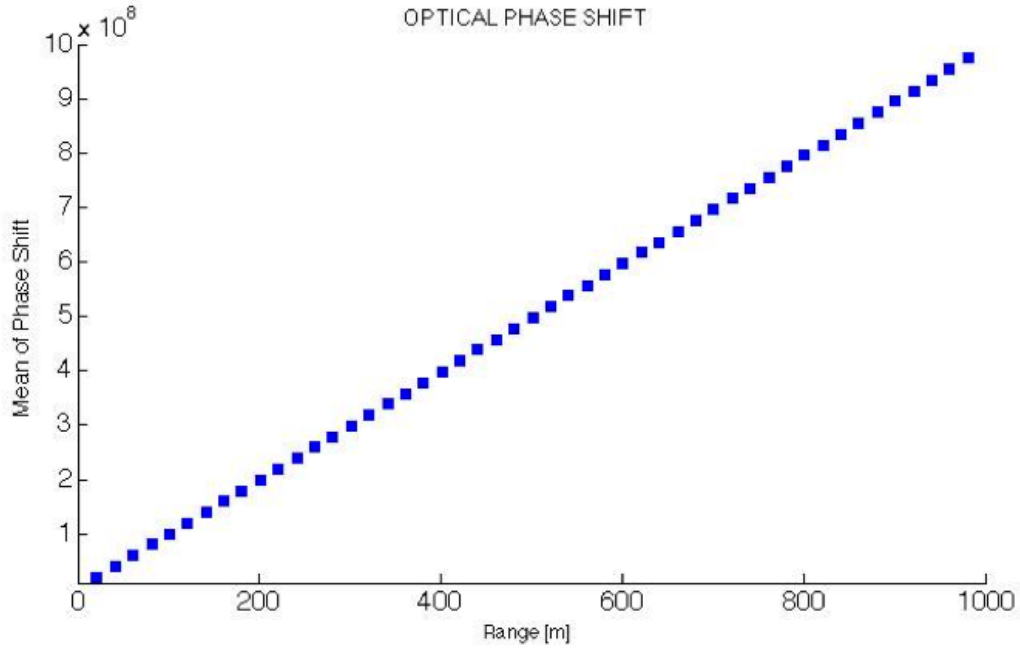

Figure 3.12. Mean Phase Shift of 1000 rays and 100 runs versus the propagation distance.

results using the following parameters: L = 1 km, $\mu_n = 1.00026$ (free-space index), $\sigma_n = 0.000016$, $numberofrays = 1000$ and $N = 1000$. The radius of the randomly selected spheres is chosen in the range of 1 mm to 1 m. The results show a linear increase of the phase shift with the propagation length.

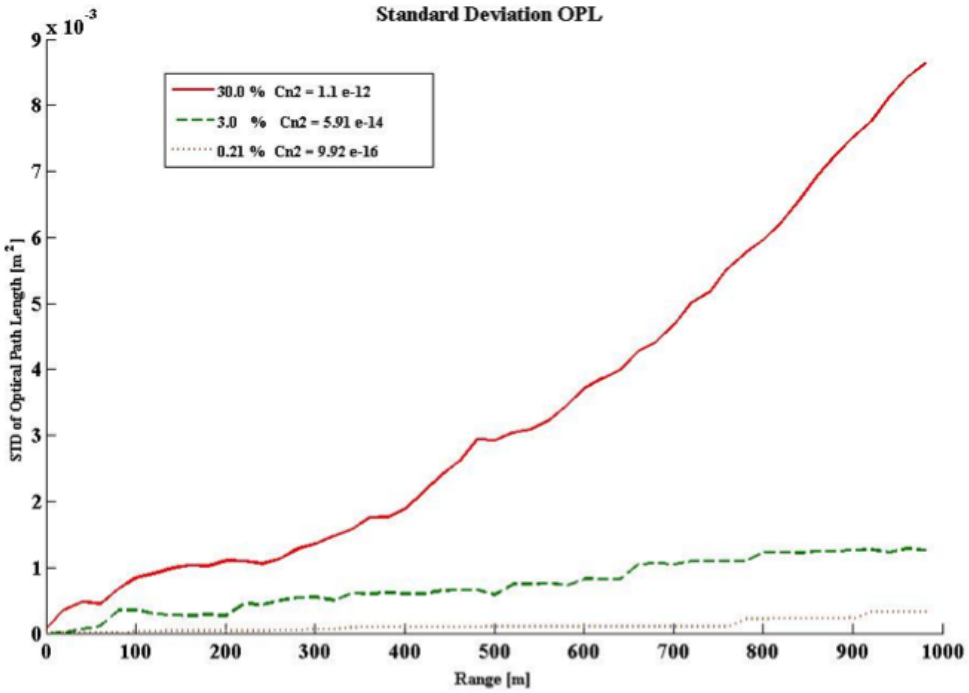

Figure 3.13. Standard Deviation of Optical Phase Shift over 1000 rays and 100 runs for different turbulence levels.

4. CONCLUSIONS

We have developed a new model to assess the effects of turbulence on laser beam propagation in Free-Space. We modeled the atmosphere along the laser beam propagation path as a spatial distribution of spherical bubbles. A Monte Carlo numerical simulation of the beam propagating through the random medium was presented. Monte Carlo simulations have proved capable of assessing beam wander, in particular the $(Range)^3$ dependence of mean square beam wander. Aperture averaging simulation results show the expected reduction of intensity fluctuations with increasing aperture diameter and quantitatively the differences in behavior between different turbulence regimes. Also, this new model has proved capable of assessing the structure of the phase fluctuations between two beams, and the results agreed well with the theoretical expression for weak turbulence. This result is remarkable because the model used was completely unrelated to the Kolmogorov model, yet yielded the same five-thirds power law dependency.

All these results are noteworthy because there are some limitations. The main limitation faced in the geometrical Monte Carlo simulations has been the limitation of the spheres coverage percentage to 30%, the Rays to 1000 and the Runs to 100. This limitation was due to the long run time, which was about 40 minutes for each choice of the bubbles' standard deviation of their refractive index fluctuations. Such a program could be further optimized to reduce run time, as well as computers with faster processing time or super computers could be used to increase the number of simulation runs. This would allow the simulation results to be smoother giving better results as well as allowing the study of more turbulence levels through a larger variation in the simulation parameters.

REFERENCES

1. Wu, Z., Y. Wei, R. Yang and L. Guo, "Study on Scintillation Considering Inner- and Outer-Scales for Laser Beam Propagation on the Slant Path Through the Atmospheric Turbulence", *Progress In Electromagnetics Research*, Vol. 80, pp. 277–293, 2008.

2. Yuksel, H., H. Meric and F. Kunter, "Study of Strong Turbulence Effects for Optical Wireless Links", *Proc. SPIE*, Vol. 8517, pp. 85170I–85170I–14, 2012.

3. Wasiczko, L. M., I. I. Smolyaninov and C. C. Davis, "Analysis of Compound Parabolic Concentrators and Aperture Averaging to Mitigate Fading on Free-Space Optical Links", *Proc. SPIE*, Vol. 5160, pp. 133–142, 2004.

4. Ishimaru, A., *Wave Propagation and Scattering in Random Media*, Wiley, 1999.

5. Yuksel, H., *Studies of the Effects of Atmospheric Turbulence on Free Space Optical Communication*, Ph.D. Thesis, University of Maryland, 2005.

6. Yuksel, H., A. Walid and C. Davis, "A Geometrical Optics Approach for Modeling Atmospheric Turbulence", *The International Society for Optics and Photonics*, Vol. 5891, 2005.

7. Andrews, L. C. and R. L. Phillips, *Laser Beam Propagation through Random Media*, The International Society for Optical Engineering, Bellingham,Washington, USA, 2005.

8. Zhang, Y., *Review of Free-Space Optical Communications with Diverging Beam*, M.S. Thesis, Michigan Technological University, 2012.

9. Qiang, X., F. Zong, J. Song, J. Zhao, Y. Li and J. Liu, "Measurement of the Inner Scale of Laboratory-Simulated Atmospheric Turbulence", *Communications*

and Photonics Conference and Exhibition (ACP), 2009 Asia, pp. 1–2, 2009.

10. Hill, R. J., "Comparison of Scintillation Methods for Measuring The Inner Scale of Turbulence", *Applied Optics*, Vol. 27, No. 11, pp. 2187–2193, 1988.

11. Livingston, P. M., "Proposed Method of Inner Scale Measurement in a Turbulent Atmosphere", *Applied Optics*, Vol. 11, No. 3, pp. 684–687, Mar 1972.

12. Chernov, L. A., *Wave propagation in a Random Medium*, McGraw-Hill, 1960.

13. Tatarskiĭ, V., *Wave Propagation in a Turbulent Medium*, Dover, 1961.

14. Wu, X., P. Liu and M. Matsumoto, "A Study on Atmospheric Turbulence Effects in Full-Optical Free-Space Communication Systems", *Wireless Communications Networking and Mobile Computing (WiCOM), 2010 6th International Conference*, pp. 1–5, 2010.

15. Matsumoto, M., K. Kazaura, P. Dat, A. Shah, K. Omae, T. Suzuki, K. Wakamori, T. Higashino, K. Tsukamoto and S. Komaki, "An Alternative Access Technology for Next Generation Networks Based on Full-Optical Wireless Communication Links", *Innovations in NGN: Future Network and Services, 2008. K-INGN 2008. First ITU-T Kaleidoscope Academic Conference*, pp. 221–228, 2008.

16. Peng, L., K. Kazaura, K. Wakamori and M. Matsumoto, "Studies on C_n^2 and Its Effects on Free Space Optical Communication System", *Information and Telecommunication Technologies (APSITT), 2010 8th Asia-Pacific Symposium on*, pp. 1–6, 2010.

17. Kaushal, H., V. Kumar, A. Dutta, H. Aennam, V. Jain, S. Kar and J. Joseph, "Experimental Study on Beam Wander Under Varying Atmospheric Turbulence Conditions", *Photonics Technology Letters, IEEE*, Vol. 23, No. 22, pp. 1691–1693, 2011.

18. Ciddor, P., *Refractive Index of Air: New Equations for the Visible and Near Infrared*, Applied Optics, Optical Society of America, 1996.

19. Morgan, B., *Elements of Simulation*, Cambridge:The University Press, 1984.

20. Churnside, J. H. and R. J. Lataitis, "Wander of an Optical Beam in the Turbulent Atmosphere", *Applied Optics*, Vol. 29, No. 7, pp. 926–930, 1990.

21. Beckmann, P., "Signal Degeneration in Laser Beams Propagated Through a Turbulent Atmosphere", *Radio Science*, Vol. 69D, No. 7, pp. 629–640, 1965.

22. Andreev, G. and E. Gelfer, "Angular Random Walks of the Center of Gravity of the Cross Section of a Diverging Light Beam", *Radiophysics and Quantum Electronics*, Vol. 14, No. 9, pp. 1145–1147, 1971.

23. Clifford, S., "The Classical Theory of Wave Propagation in a Turbulent Medium", Vol. 25, pp. 9–43, 1978.